Ultrasonics Sonochemistry 22 (2015) 51–58

Contents lists available at ScienceDirect

Ultrasonics Sonochemistry

journal homepage: www.elsevier.com/locate/ultson

A method for predicting the number of active bubbles in sonochemical reactors

Slimane Merouani [a,b], Hamza Ferkous [a], Oualid Hamdaoui [a,*], Yacine Rezgui [c], Miloud Guemini [c]

[a] Laboratory of Environmental Engineering, Department of Process Engineering, Faculty of Engineering, Badji Mokhtar – Annaba University, P.O. Box 12, 23000 Annaba, Algeria
[b] Department of Chemical Engineering, Faculty of Pharmaceutical Engineering Process, University of Constantine 3, Constantine, Algeria
[c] Laboratory of Applied Chemistry and Materials Technology, University of Oum El-Bouaghi, P.O. Box 358, 04000 Oum El Bouaghi, Algeria

ARTICLE INFO

Article history:
Received 26 February 2014
Received in revised form 13 June 2014
Accepted 21 July 2014
Available online 27 July 2014

Keywords:
Number of bubbles
Ultrasonic reactors
Bubble dynamics
Chemical kinetics
Sonochemistry
Ultrasonic frequency

ABSTRACT

Knowledge of the number of active bubbles in acoustic cavitation field is very important for the prediction of the performance of ultrasonic reactors toward most chemical processes induced by ultrasound. The literature in this field is scarce, probably due to the complicated nature of the phenomena. We introduce here a relatively simple semi-empirical method for predicting the number of active bubbles in an acoustic cavitation field. By coupling the bubble dynamics in an acoustical field with chemical kinetics occurring in the bubble during oscillation, the amount of the radical species ·OH and $HO_2^{\cdot}$ and molecular H_2O_2 released by a single bubble was estimated. Knowing that the H_2O_2 measured experimentally during sonication of water comes from the recombination of hydroxyl (·OH) and perhydroxyl ($HO_2^{\cdot}$) radicals in the liquid phase and assuming that in sonochemistry applications, the cavitation is transient and the bubble fragments at the first collapse, the number of bubbles formed per unit time per unit volume is then easily determined using material balances for H_2O_2, ·OH and $HO_2^{\cdot}$ in the liquid phase. The effect of ultrasonic frequency on the number of active bubbles was examined. It was shown that increasing ultrasonic frequency leads to a substantial increase in the number of bubbles formed in the reactor.

1. Introduction

Ultrasound has a wide variety of applications, ranging from the degradation of pollutants [1–3], polymerization reactions [4] and fabrication of nano-particles [5,6] to food science [7,8] and biomedical applications [9,10]. Most of these processes arise from acoustic cavitation, that is, the formation, growth and violent collapse of microscopic bubbles as the alternate compressions and rarefactions of the sound waves propagate through the liquid [11]. Acoustic cavitation is also responsible for the emission of broad wavelength light, which is called sonoluminescence (SL) [12,13]. The microbubbles can be either stable, oscillating about their average or equilibrium size for many acoustic cycles or transient when they grow to a certain size in one or at most a few acoustic cycles and violently collapse during the compression part of the wave [14]. Sonochemistry and sonoluminescence are attributed to the transient cavitation bubbles [14].

The chemical effects of acoustic cavitation are a direct result of the very high temperatures, of the order of 5000 K, and pressures, in the range of hundreds of bars, which are reached in the bubbles when they collapse [15,16]. The extremely high conditions formed in collapsing bubbles in aqueous solutions lead to the thermal dissociation of the trapped water vapor into reactive hydroxyl radicals (·OH) and hydrogen atoms (H·) [17]. These active species can recombine, react with other gaseous species present in the cavity to form other active species such as $HO_2^{\cdot}$ and O, or diffuse out of the bubble into the bulk liquid medium where they are able to induce chemical transformation [18]. In the absence of any solutes in the liquid medium, these primary active species of sonolysis mostly recombine at the bubble solution interface to form hydrogen peroxide (H_2O_2) that is released in the medium according to the following reactions [19]:

$$2\cdot OH \rightarrow H_2O_2 \quad k_1 = 5.5 \times 10^9\ M^{-1}\ s^{-1} \tag{1}$$

$$2\cdot OOH \rightarrow H_2O_2 + O_2 \quad k_2 = 8.3 \times 10^5\ M^{-1}\ s^{-1} \tag{2}$$

Due to their high reactivity and their short lifetime, the total number of primary active species produced by the acoustic bubbles cannot be directly measured. It is generally accepted that the yield of H_2O_2 can be considered as an indicator for quantifying the overall chemical yield of ultrasound in aqueous media [20,21].

* Corresponding author. Tel./fax: +213 38876560.
E-mail addresses: ohamdaoui@yahoo.fr, oualid.hamdaoui@univ-annaba.dz (O. Hamdaoui).

http://dx.doi.org/10.1016/j.ultsonch.2014.07.015
1350-4177/

Nomenclature

c	speed of sound in the liquid medium (m s^{-1})
f	frequency of ultrasonic wave (Hz)
I_a	acoustic intensity of ultrasonic irradiation (W m^{-2})
I	number of chemical reactions
K	number of all species in the bubble
N	number of bubbles collapsing per unit volume per unit time (L^{-1} s^{-1})
n_{H_2O}	number of moles of H_2O in the bubble (mol)
nt	Number of moles of all species in the bubble (mol)
$n_{H_2O_2}$	number of moles of H_2O_2 released by the collapse of single bubble (mol)
$n_{\cdot OH}$	number of moles of ·OH released by the collapse of single bubble (mol)
$n_{HO_2^{\cdot}}$	number of moles of $HO_2^{\cdot}$ released by the collapse of single bubble (mol)
p	pressure inside a bubble (Pa)
p_∞	ambient static pressure (Pa)
P_A	amplitude of the acoustic pressure (Pa)
P_v	vapor pressure of water (Pa)
P_{g0}	initial gas pressure (Pa)
R	radius of the bubble (m)
R_{max}	maximum radius of the bubble (m)
R_{min}	minimum radius of the bubble at the collapse (m)
R_0	ambient bubble radius (m)
$r_{H_2O_2}$	production rate of H_2O_2 (mol s^{-1})
$r_{\cdot OH}$	production rate of ·OH (mol s^{-1})
$r_{HO_2^{\cdot}}$	production rate of $HO_2^{\cdot}$ (mol s^{-1})
t	time (s)
T	temperature inside a bubble (K)
T_∞	ambient liquid temperature (K)
V	volume of the bubble (m^3)
X	symbol of chemical species

Greek letters

γ	specific heat ratio (c_p/c_v) of the gas mixture
σ	surface tension of liquid water (N m^{-1})
ρ	density of liquid water (kg m^{-3})
μ	viscosity of liquid water (N m^{-2} s)
ε	molar extinction coefficient of I_3^- (L mol^{-1} cm^{-1})

The light emission from acoustic bubbles (SL) arises essentiely from vibronically excited states of species, i.e. ·OH radicals, produced as a result of the high temperatures and pressures that are generated within the core of bubbles during strong collapse [22].

The overall efficiency of sonochemical processes depends on the bubble population (bubbles number and sizes), which in turn depend upon various parameters, such as the ultrasonic frequency and acoustic amplitude [23]. Knowledge of the bubbles number and sizes is very important for the prediction of the performance of ultrasonic reactors. The literature in this field is scarce, probably due to complicated nature of the phenomena. In our previous work [24], we have studied theoretically the effect of ultrasonic frequency and acoustic amplitude on the size of sonochemically active bubbles using a model that combines the dynamics of bubble oscillation in acoustical field with chemical kinetics occurring in the bubble during its oscillation. In this work, basing on our theoretical model developed earlier for a single bubble [24], we introduce a relatively simple semi-empirical method for predicting the number of active bubbles in a sonochemical reactor. The effect of ultrasonic frequency on the number of bubbles formed in the sonochemical reactor was examined.

2. Materials and methods

2.1. Ultrasonic reactor

Sonolysis experiments were conducted in cylindrical water-jacketed glass reactors (Fig. 1). The ultrasonic waves of 300 kHz were emitted from the bottom of the reactor through a piezoelectric disc (diameter 4 cm) fixed on Pyrex plate (diameter 5 cm). The ultrasonic waves of 585, 860 and 1140 kHz were delivered from the bottom through a Meinhardt multifrequency transducer (model E/805/T/M, diameter of the active area 5.3 cm). The temperature of the solution was monitored using a thermocouple immersed in the reacting medium. Acoustic power dissipated in the reactor was estimated using a standard calorimetric method [25,26].

2.2. Procedures

Sonochemical experiments involving H_2O_2 production were performed by sonicating 300 mL of distilled water. The temperature of the aerated solution was maintained at 25 °C by circulating cooling water through a jacket surrounding the cell. The acoustic power delivered to the reactor was adjusted calorimetrically to obtain the same value of acoustic intensity, 2 W cm^{-2} (corresponding to an acoustic amplitude of 1.73 atm), for all frequencies.

Hydrogen peroxide concentrations were analytically determined using the iodometric method [27]. Sample aliquots taken periodically from the reactor during sonolysis were added in the quartz cell of the spectrophotometer containing 1 mL of potassium iodide (0.1 M) and 20 μL of ammonium heptamolybdate (0.01 M). The iodide ion (I^-) reacts with H_2O_2 to form the triiodide ion (I_3^-). The mixed solutions were allowed to stand for 5 min before absorbance was measured. The absorbance was recorded with a UV–visible spectrophotometer (Lightwave II) at the maximum wavelength of the formed triiodide (I_3^-) (352 nm; the molar absorptivity ε = 26300 L mol^{-1} cm^{-1}).

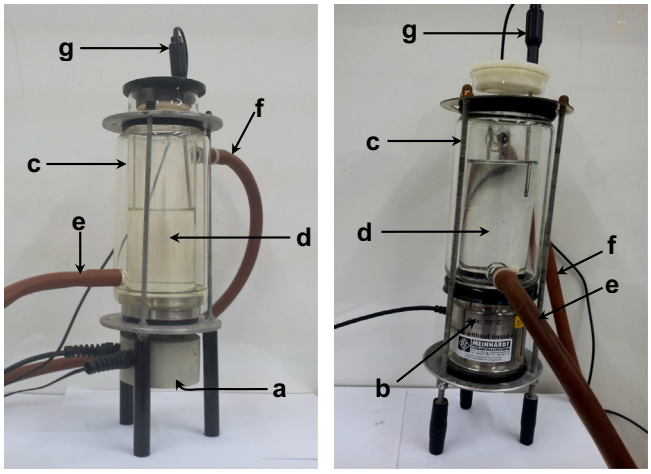

Fig. 1. Sonochemical realtors used for quantifying the amount of H_2O_2 formed in the liquid water during sonication. (a) 300 kHz ultrasonic transducer, (b) Meinhardt multi-frequency transducer operating at 585, 860 and 1140 kHz, (c) cylindrical jacketed glass cells, (d) sonicated water, (e) inlet cooling water, (f) outlet cooling water, (g) thermocouples.

3. Model and computational methods

The theoretical model used in this study and the assumptions therein have been fully described in our previous papers [24,28–30]. The model combines the dynamics of single bubble with chemical kinetics occurring inside a bubble during the collapse. The following is a brief description of the model.

3.1. Bubble dynamics model

A gas and vapor filled spherical bubble isolated in water oscillates under the action of a sinusoidal sound wave. The temperature and pressure in the bubble are assumed spatially uniform and the gas content of the bubble behaves as an ideal gas [31]. The radial dynamics of the bubble is described by a model furnished by the Keller-Miksis equation that includes first order terms in the Mach number ($\dot{R}/c$) [32,33]:

$$\left(1-\frac{\dot{R}}{c}\right)R\ddot{R}+\frac{3}{2}\left(1-\frac{\dot{R}}{3c}\right)\dot{R}^2 = \frac{1}{\rho_L}\left(1+\frac{\dot{R}}{c}+\frac{R}{c}\frac{d}{dt}\right)\left[p-p_\infty-\frac{2\sigma}{R}-4\mu\frac{\dot{R}}{R}+P_A\sin(2\pi ft)\right] \quad (3)$$

In this equation dots denote time derivatives (d/dt), R is the radius of the bubble, c is the speed of sound in the liquid, ρ_L is the density of the liquid, σ is the surface tension, μ is the liquid viscosity, p is the pressure inside the bubble, p_∞ is the ambient static pressure, P_A is the acoustic amplitude and f is the sound frequency. The acoustic amplitude P_A is correlated with the acoustic intensity I_a, or acoustic power per unit area, as $P_A = (2I_a\rho_L c)^{1/2}$ [16]. Eq. (3) is only accurate to first order in the bubble wall Mach number ($\dot{R}/c$) but, for all acoustic amplitudes in this study, this level of accuracy is sufficient (the speed of the bubble wall ($|\dot{R}|$) at the collapse never exceeds the sound velocity in the liquid c, which is the assumption used in the derivation of the equation [33]).

In the present model, the expansion of the bubble is assumed as isothermal and its total compression is considered as adiabatic [34,35]. These assumptions are widely accepted since the lifetime of a bubble oscillating at high frequency is relatively short with a very rapidly occurring collapse event. We also assume that the vapor pressure in the bubble remains constant during the bubble expansion phase and there is no gas diffusion during expansion and no mass and heat transfer of any kind during collapse. We noticed here that Storey and Szeri [36] demonstrated that the inclusion of non-equilibrium phase change of water vapor at the bubble wall has practically no effect on the maximum bubble temperature attained in the bubble at the collapse when the compression ratio of the bubble (R_{max}/R_{min}) is less than 20 (R_{max} is the maximum bubble radius and R_{min} is the minimum bubble radius). This level of R_{max}/R_{min} was rarely attained in the present numerical study. Therefore, in order to reduce computational parameters, the current model takes, as input, initial bubble vapor content and neglects mass and heat transfer during bubble expansion and collapse.

Based on the above assumptions, the temperature inside the bubble at any instant during the implosion phase can be calculated from the bubble size, using the adiabatic law [30]:

$$T = T_\infty\left(\frac{R_{max}}{R}\right)^{3(\gamma-1)} \quad (4)$$

where T_∞ is the bulk liquid temperature and γ is the ratio of specific heat capacities (c_p/c_v) of the vapor/gas mixture. It is important to notice here that the assumption of spatial uniform pressure and temperature inside the bubble is valid as long as inertia effects are negligible and the velocity of the bubble wall is below the speed of sound in the vapor/gas mixture. This assumption was justified in detail in the paper published by Kamath et al. [37].

3.2. Chemical kinetics model

For a bubble initially composed of oxygen (or air) and water vapor, a kinetic mechanism consisting of series of reversible chemical reactions (25 chemical reactions for O_2 bubble [29,34,37] and 73 reactions for air bubble [38–40]) which take place inside a bubble at high temperatures is taken into account. The reaction schemes involve the species O_2, H_2O, $^{\cdot}OH$, $H^{\cdot}$, O, $HO_2^{\cdot}$, H_2O_2, O_3 and H_2 for O_2 bubble and O_2, N_2, H_2O, $^{\cdot}OH$, $H^{\cdot}$, O, $HO_2^{\cdot}$, O_3, H_2, H_2O_2, N, NO, NO_2, NO_3, HNO_2, HNO_3, N_2O, HNO, NH, NH_2, NH_3, N_2H_2, N_2H_3, N_2H_4, N_2O_4 and N_2O_5 for air bubble.

The chemical kinetics model consists of the reaction mechanism and determines the production of each species during the bubble collapse. Rate expressions for the chemical reactions consider elementary reversible reactions involving K chemical species, which can be represented in the general form as [41]

$$\sum_{k=1}^{K}\upsilon'_{ki}\,X_k \;\leftrightarrow\; \sum_{k=1}^{K}\upsilon''_{ki}\,X_k \quad (5)$$

in which υ_{ki} is the stoichiometric coefficients of the ith reaction and X_k is the chemical symbol for the kth species. K is the number of species. The superscript $'$ indicates forward stoichiometric coefficients, while $''$ indicates reverse stoichiometric coefficients. The production rate w_k of the kth species can be written as a summation of the rate of the variables for all reactions involving the kth species [41]:

$$w_k = \sum_{i=1}^{I}(\upsilon''_{ki}-\upsilon'_{ki})r_i \quad (k=1,\ldots,K,\ i=1,\ldots,I) \quad (6)$$

where I is the number of reactions. The rate r_i for the ith reaction is given by the difference of the forward and reverse rates as [41]

$$r_i = k_{f_i}\prod_{k=1}^{K}[X_k]^{\upsilon'_{ki}} - k_{r_i}\prod_{k=1}^{K}[X_k]^{\upsilon''_{ki}} \quad (7)$$

where $[X_k]$ is the molar concentration of the kth species and k_{fi} and k_{ri} are the forward and reverse rate constants of the ith reaction, respectively. The forward and reverse rate constants for the ith reaction are assumed to have the following Arrhenius temperature dependence [39–42]:

$$k_{f_i} = A_{f_i}\,T^{b_{f_i}}\exp\left(-\frac{E_{a_{fi}}}{R_gT}\right) \quad (8)$$

$$k_{r_i} = A_{r_i}\,T^{b_{ri}}\exp\left(-\frac{E_{a_{ri}}}{R_gT}\right) \quad (9)$$

where R_g is the universal gas constant, A_{fi} (A_{ri}) is the pre-exponential factor, b_{fi} (b_{ri}) is the temperature exponent and E_{fi} (E_{ri}) is the activation energy. The rate constants of the important reactions, listed in Table 1 for O_2 bubble and Table 2 for air bubble, were obtained from the NIST Chemical Kinetics Database [43] and other bibliographic references [34,37–40,44].

3.3. Procedure of the numerical simulation

The Keller-Miksis equation (Eq. (3)), describing the dynamics of the bubble, is a non-linear second-order differential equation which requires an approximate numerical method of solution. Eq. (3) can be reduced to a system of two first-order differential equations

Table 1
The important chemical reactions inside a collapsing O_2/water vapor bubble [29,34,37,43,44] when the maximum bubble temperature is 5100 K, which is the temperature obtained at 200 kHz under the experiment conditions of Jiang et al. [63]. M is the third body. Subscript "*f*" denotes the forward reaction and "*r*" denotes the reverse reaction. *A* is in ($cm^3\ mol^{-1}\ s^{-1}$) for two body reaction [($cm^6\ mol^{-2}\ s^{-1}$) for a three body reaction], and E_a is in ($cal\ mol^{-1}$).

N°	Chemical reaction	A_f	b_f	E_{af}	A_r	b_r	E_{ar}
1	$H_2O + M \leftrightarrow H^{\cdot} + {}^{\cdot}OH + M$	1.912×10^{23}	−1.83	1.185×10^5	2.2×10^{22}	−2.0	0.0
2	$O_2 + M \leftrightarrow O + O + M$	4.515×10^{17}	−0.64	1.189×10^5	6.165×10^{15}	−0.5	0.0
3	$H_2O + O \leftrightarrow {}^{\cdot}OH + {}^{\cdot}OH$	2.97×10^6	2.02	1.34×10^4	1.465×10^5	2.11	-2.904×10^3
4	$H^{\cdot} + O_2 + M \leftrightarrow HO_2^{\cdot} + M$	1.475×10^{12}	0.6	0.0	3.09×10^{12}	0.53	4.887×10^4
5	$H^{\cdot} + {}^{\cdot}OH \leftrightarrow O + H_2$	2.667×10^4	2.65	4.88×10^3	3.82×10^{12}	0.0	7.948×10^3
6	$H^{\cdot} + H_2O \leftrightarrow {}^{\cdot}OH + H_2$	2.298×10^9	1.40	1.832×10^4	2.16×10^8	1.52	3.45×10^3
7	$HO_2^{\cdot} + O \leftrightarrow {}^{\cdot}OH + O_2$	3.25×10^{13}	0.0	0.0	3.252×10^{12}	0.33	5.328×10^4
8	$HO_2^{\cdot} + H^{\cdot} \leftrightarrow {}^{\cdot}OH + {}^{\cdot}OH$	7.079×10^{13}	0.0	2.95×10^2	2.027×10^{10}	0.72	3.684×10^4
9	$H_2O + HO_2^{\cdot} \leftrightarrow H_2O_2 + {}^{\cdot}OH$	1.838×10^{10}	0.59	3.089×10^4	1.0×10^{12}	0.0	0.0
10	${}^{\cdot}OH + HO_2^{\cdot} \leftrightarrow H_2O_2 + O$	8.66×10^3	2.68	1.856×10^4	9.550×10^6	2.0	3.97×10^3
11	$HO_2^{\cdot} + H^{\cdot} \leftrightarrow H_2 + O_2$	1.66×10^{13}	0.0	8.23×10^2	3.164×10^{12}	0.35	5.551×10^4
12	${}^{\cdot}OH + {}^{\cdot}OH + M \leftrightarrow H_2O_2 + M$	1.0×10^{14}	−0.37	0.0	2.951×10^{14}	0.0	4.843×10^4
13	$HO_2^{\cdot} + HO_2^{\cdot} \leftrightarrow H_2O_2 + O_2$	4.2×10^{14}	0.0	1.198×10^4	4.634×10^{16}	−0.35	5.067×10^4

Table 2
The important chemical reactions inside a collapsing air/water vapor bubble [38–40,43,44] when the maximum bubble temperature is 4800 K, which the temperature obtained at 300 kHz under our experimental conditions. M is the third body. Subscript "*f*" denotes the forward reaction and "*r*" denotes the reverse reaction. *A* is in ($cm^3\ mol^{-1}\ s^{-1}$) for two body reaction [($cm^6\ mol^{-2}\ s^{-1}$) for a three body reaction], and E_a is in ($cal\ mol^{-1}$).

N°	Chemical reaction	A_f	b_f	E_{af}	A_r	b_r	E_{ar}
1	$H_2O + M \leftrightarrow H^{\cdot} + {}^{\cdot}OH + M$	1.912×10^{23}	−1.83	1.185×10^5	2.2×10^{22}	−2.0	0.0
2	$O_2 + M \leftrightarrow O + O + M$	4.515×10^{17}	−0.64	1.189×10^5	6.165×10^{15}	−0.5	0.0
3	$H^{\cdot} + O_2 \leftrightarrow O + {}^{\cdot}OH$	1.915×10^{14}	0.0	1.644×10^4	5.481×10^{11}	0.39	-2.93×10^2
4	$H^{\cdot} + O_2 + M \leftrightarrow HO_2^{\cdot} + M$	1.475×10^{12}	0.6	0.0	3.09×10^{12}	0.53	4.887×10^4
5	$O + H_2O \leftrightarrow {}^{\cdot}OH + {}^{\cdot}OH$	2.97×10^6	2.02	1.34×10^4	1.465×10^5	2.11	-2.904×10^3
6	$HO_2^{\cdot} + O \leftrightarrow {}^{\cdot}OH + O_2$	3.25×10^{13}	0.0	0.0	3.252×10^{12}	0.33	5.328×10^4
7	$O + H_2 \leftrightarrow H^{\cdot} + {}^{\cdot}OH$	3.82×10^{12}	0.0	7.948×10^3	2.667×10^4	2.65	4.88×10^3
8	$H^{\cdot} + H_2O \leftrightarrow {}^{\cdot}OH + H_2$	2.298×10^9	1.40	1.832×10^4	2.16×10^8	1.52	3.45×10^3
9	$H_2O + HO_2^{\cdot} \leftrightarrow H_2O_2 + {}^{\cdot}OH$	1.838×10^{10}	0.59	3.089×10^4	1.0×10^{12}	0.0	0.0
10	${}^{\cdot}OH + {}^{\cdot}OH + M \leftrightarrow H_2O_2 + M$	2.951×10^{14}	0.0	4.843×10^4	1.0×10^{14}	−0.37	0.0
11	$HO_2^{\cdot} + HO_2^{\cdot} \leftrightarrow H_2O_2 + O_2$	4.2×10^{14}	0.0	1.198×10^4	4.634×10^{16}	−0.35	5.067×10^4
12	$O + N_2 \leftrightarrow NO + N$	7.60×10^{13}	0.0	7.60×10^4	1.60×10^{13}	0.0	0.00
13	$NO + HO_2^{\cdot} \leftrightarrow OH + NO_2$	3.0×10^{12}	0.5	2.4×10^3	1.0×10^{11}	0.5	1.2×10^4
14	$NO_2 + M \leftrightarrow O + NO + M$	1.1×10^{16}	0.0	6.6×10^4	1.1×10^{15}	0.0	-1.88×10^3
15	$NO_2 + NO_2 \leftrightarrow NO + NO_3$	3.90×10^{11}	0.0	2.400×10^4	4.1×10^{14}	0.0	9.62×10^2
16	$NO_2 + O + M \leftrightarrow NO_3 + M$	1.1×10^{19}	0.0	0.0	2.5×10^9	0.0	0.0
17	$NO_3 + H \leftrightarrow OH + NO_2$	3.5×10^{14}	0.0	1.5×10^3	–	–	–
18	$OH + NO + M \leftrightarrow HNO_2 + M$	8.0×10^{15}	0.0	-1.0×10^3	5.10×10^{17}	−1.0	5.000×10^4
19	$HNO_2 + H \leftrightarrow H_2 + NO_2$	4.9×10^{11}	0.5	3.00×10^3	2.40×10^{13}	0.0	2.90×10^4
20	$O + HNO_2 \leftrightarrow HNO + O_2$	3.0×10^{12}	0.0	1.60×10^4	–	–	–
21	$HNO + M \leftrightarrow H + NO + M$	3.0×10^{16}	0.0	4.9×10^4	5.4×10^{15}	0.0	-3.0×10^2
22	$HNO + O \leftrightarrow OH + NO$	4.9×10^{11}	0.5	2.0×10^3	–	–	–
23	$HNO + OH \leftrightarrow NO + H_2O$	6.3×10^{13}	0.0	0.0	2.40×10^6	0.0	5.0×10^3
24	$OH + NO_2 + M \leftrightarrow HNO_3 + M$	5.0×10^{17}	0.0	0.0	1.6×10^{15}	0.0	3.08×10^4

$$\frac{dR}{dt} = \dot{R} \tag{10}$$

$$\frac{d\dot{R}}{dt} = \frac{\frac{1}{\rho_L}\left(1 + \frac{\dot{R}}{c} + \frac{R}{c}\frac{d}{dt}\right)\left[p - p_\infty - \frac{2\sigma}{R} - 4\mu\frac{\dot{R}}{R} + P_A \sin(2\pi f t)\right] - \frac{3}{2}\left(1 - \frac{\dot{R}}{3c}\right)\dot{R}^2}{\left(1 - \frac{\dot{R}}{c}\right)R} \tag{11}$$

The system of Eqs. (10) and (11) was solved by the fourth-order Runge-Kutta method using the following initial conditions:

$$\text{At } t = 0,\ R = R_0 \text{ and } \dot{R} = 0$$

where R_0 is the ambient bubble radius.

As the expansion of the bubble is isothermal and the subsequent collapse is adiabatic, the pressure inside a bubble (p) is expressed as [30]

- Expansion phase $(R_0 \leqslant R \leqslant R_{max} \text{ and } dR/dt \geqslant 0)$:

$$p = P_v + P_{g0}\left(\frac{R_0}{R}\right)^3 \tag{12}$$

- Collapse phase $(R_{min} \leqslant R \leqslant R_{max} \text{ and } dR/dt \leqslant 0)$:

$$p = \left[P_v + P_{g0}\left(\frac{R_0}{R_{max}}\right)^3\right]\left(\frac{R_{max}}{R}\right)^{3\gamma} \tag{13}$$

where P_v is the saturated vapor pressure, $P_{g0} = p_\infty + (2\sigma/R_0) - P_v$ is the gas pressure in the bubble at its ambient state ($R = R_0$). The transition from isothermal expansion to adiabatic collapse occurs when the bubble wall velocity dR/dt change the sign from positive to negative at around the maximum bubble radius (R_{max}).

Several physical properties (saturated vapor pressure, density, surface tension, viscosity and sound velocity) in the above equations change with the liquid temperature T_∞ (water is the liquid medium in this study). The equations for the physical properties of water have been described in our previous work [28].

The simulation of the chemical reactions in the bubble (25 chemical reactions for the case of an O_2-bubble and 73 chemical reactions for the case of air bubble) starts at the beginning of the adiabatic phase (at time corresponding to $R = R_{max}$). The application of Eq. (6) for all species involved in the used chemical kinetics mechanism (10 species for O_2-bubble and 26 species for air-bubble)

gives two systems of ordinary differential equations (10 equations for the case of O_2-bubble and 26 equations for the case of air-bubble). For example, according to Table 1, the application of Eq. (6) to the H_2O species gives:

$$w_{H_2O} = \frac{1}{V}\frac{dn_{H_2O}}{dt} = -\{k_{f1}[H_2O]\,[M] - k_{r1}[H^{\cdot}]\,[^{\cdot}OH]\,[M]\} - \{k_{f3}\,[H_2O]\,[O] - k_{r3}\,[^{\cdot}OH]^2\} - \{k_{f6}\,[H_2O]\,[H] - k_{r6}\,[H_2]\,[^{\cdot}OH]\} - \{k_{f9}\,[H_2O]\,[HO_2^{\cdot}] - k_{r9}\,[H_2O_2][^{\cdot}OH]\} \quad (14)$$

when V is the volume of the bubble and n_{H_2O} is the number of moles of H_2O.

Using the ideal gas law $PV = n_tRT$, Eq. (14) can be rewritten as

$$\frac{dn_{H_2O}}{dt} = -\frac{ntRT}{p}\left\langle \begin{array}{l} \{k_{f1}\,[H_2O]\,[M] - k_{r1}\,[H^{\cdot}]\,[^{\cdot}OH]\,[M]\} + \{k_{f3}\,[H_2O]\,[O] - k_{r3}[^{\cdot}OH]^2\} - \\ \{k_{f6}\,[H_2O]\,[H] - k_{r6}\,[H_2]\,[^{\cdot}OH]\} + \{k_{f9}\,[H_2O]\,[HO_2^{\cdot}] - k_{r9}\,[H_2O_2]\,[^{\cdot}OH]\} \end{array}\right\rangle \quad (15)$$

where n_t is number of moles of all species present in the bubble.

The input parameters for solving the system of ordinary differential equations obtained by Eq. (6) are the composition of water vapor and other gases in the bubble at time corresponding to $R = R_{max}$, the temperature and pressure profiles in the bubble during the adiabatic phase and the collapse time. These parameters are obtained by solving the dynamics equation (Eq. (3)). As the bubble temperature increases during the adiabatic phase, the reaction system evolves and radicals start to form by thermal dissociation of H_2O and other molecules in the bubble. Thus, the composition of all species expected to be present in the bubble was determined at any temperature during the collapse period by solving the system of the ordinary differential equations obtained by Eq. (6). The system of the ordinary differential equations was solved by the finite difference method. The computer simulation of the reactions system was stopped after the end of the bubble collapse.

3.4. Determination of the number of collapsing bubbles

Firstly, it is important to mention that the phenomenon of bubble collapse and subsequent fragmentation depends on many factors such as the surface instability, local flow conditions and the bubble population in the vicinity of the bubble [45]. We assume that in sonochemistry applications, the cavitation is transient and the bubble breaks apart (fragments) at the first collapse (when the minimum bubble radius being reached) after an initial expansion. Based on these assumptions, our model described in Section 3 was used to predict the amount of the active species accumulated inside a bubble during collapse. When the end of the bubble collapse is reached, the bubble breaks apart and we assume that the bubble contents mix directly with the liquid phase surrounding the bubble [46].

On the other hand, knowing that the H_2O_2 content measured experimentally during sonication of water come essentially from the recombination of hydroxyl ($^{\cdot}OH$) and perhydroxyl ($HO_2^{\cdot}$) at the bubble solution interface according to reactions (1) and (2), the material balance equations for H_2O_2, $^{\cdot}OH$ and $HO_2^{\cdot}$ in the liquid phase (water) give the production rates of these species as

$$r_{H_2O_2} = \frac{d[H_2O_2]}{dt} = N \times n_{H_2O_2} + k_1[^{\cdot}OH]^2 + k_2[HO_2^{\cdot}]^2 \quad (16)$$

$$r_{^{\cdot}OH} = \frac{d[^{\cdot}OH]}{dt} = N \times n_{^{\cdot}OH} - 2k_1[^{\cdot}OH]^2 \quad (17)$$

$$r_{HO_2^{\cdot}} = \frac{d[HO_2^{\cdot}]}{dt} = N \times n_{HO_2^{\cdot}} - 2k_2[HO_2^{\cdot}]^2 \quad (18)$$

where N is the number of bubbles collapsing per unit volume per unit time, $n_{H_2O_2}$, $n_{^{\cdot}OH}$ and $n_{HO_2^{\cdot}}$ are the number of moles of H_2O_2, $^{\cdot}OH$ and $HO_2^{\cdot}$, respectively, released by each bubble when it collapses and k_1 and k_2 are the rate constants of reactions (1) and (2) respectively.

Since free radicals have very short lifetimes of micro- or nanoseconds [47], i.e. 1 ns for $^{\cdot}OH$ [47], steady state conditions can be assumed for $^{\cdot}OH$ and $HO_2^{\cdot}$ ($r_{^{\cdot}OH} = r_{HO_2^{\cdot}} = 0$) [48], which leads to:

$$k_1[^{\cdot}OH]^2 = \frac{1}{2}N \times n_{^{\cdot}OH} \quad (19)$$

$$k_2[HO_2^{\cdot}]^2 = \frac{1}{2}N \times n_{HO_2^{\cdot}} \quad (20)$$

Substituting expressions (19) and (20) in (16) and rearranging the equation, we obtain:

$$N = \frac{r_{H_2O_2}}{n_{H_2O_2} + 0.5(n_{^{\cdot}OH} + n_{HO_2^{\cdot}})} \quad (21)$$

In this equation, the production rate of H_2O_2, $r_{H_2O_2}$, is determined experimentally according to Section 4.1 and the number of moles $n_{H_2O_2}$, $n_{^{\cdot}OH}$ and $n_{HO_2^{\cdot}}$ released by each bubble at the end of the collapse are estimated using the model, as illustrated in Section 4.2. We notice that all these entities are strongly sensitive on operational conditions such as ultrasonic frequency, type of dissolved gas, physicochemical properties of liquid medium, surrounding pressure field in the ultrasonic reactor and operating liquid temperature (Section 4.1 showed the dependence of $r_{H_2O_2}$ on the frequency and Ref. [28] showed the sensitivity of $n_{H_2O_2}$, $n_{^{\cdot}OH}$ and $n_{HO_2^{\cdot}}$ on the operational conditions). Thus, the number of bubbles N depends strongly on the operating parameters of the sonication. It should be mentioned here that an analogous strategy for determining the number of bubbles have been used by Prasad Naidu et al. [46] using the sono-oxidation of KI solution as means.

4. Results and discussion

4.1. H_2O_2 production during water sonolysis

The iodometric method is commonly used for quantifying the amount of H_2O_2 generated during the sonication of water. Hydrogen peroxide can oxidize iodide ions and generate molecular iodine (reaction 22). In the presence of excess of iodide ions, molecular iodine form the complex I_3^- (reaction 23). Using the absorption and molar extinction coefficient, ε, the amount of hydrogen peroxide generated by sonication can be quantified.

$$H_2O_2 + 2I^- \rightarrow I_2 + 2OH^- \quad (22)$$

$$I_2 + I^- \rightarrow I_3^- \quad (23)$$

In this study, experiments were carried out at different frequencies (300, 585, 860 and 1140 kHz) when the acoustic energy dissipated to the solution and the liquid temperature were maintained constant at 2 W cm^{-2} and 25 °C respectively. For each experiment, the concentration of H_2O_2 in the sonicated medium increased linearly with sonication time (data not shown), while the rate of production remained constant. This linear increase in the sonochemical activity is generally expected as the sonication time corresponds to a linear increase in the power input. The obtained production rates of H_2O_2 with respect to the frequency are 2.5071, 4.2060, 3.4386 and 2.0960 μM min^{-1} for respectively 300, 585, 860 and 1140 kHz. Thus, an optimum frequency of 585 kHz is obtained for the production of H_2O_2. An increase in the H_2O_2 yield is observed with an increase in ultrasound frequency from 300 to 585 kHz. However, a further increase in the ultrasound frequency resulted in a decrease of H_2O_2 yield. It is

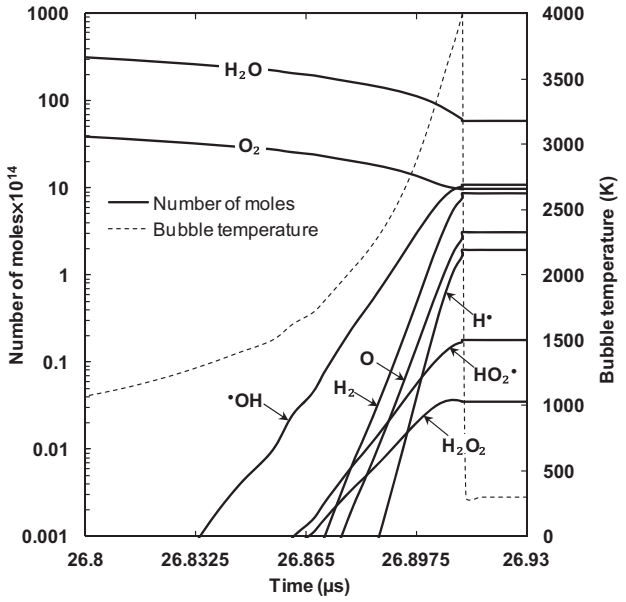

Fig. 2. Evolution of the reaction system inside a bubble as function of time at around the end of the bubble collapse (conditions: ultrasonic frequency: 21.4 kHz, acoustic amplitude: 1.31 atm, static pressure: 1 atm, liquid temperature: 21 °C, ambient bubble radius R_0: 8 μm). The principal vertical axis is in logarithmic scale. The horizontal axis is only for 0.13 μs. The numerical simulation of chemical reactions was conducted for a bubble initially composed of oxygen and water vapor.

known that an increase in the ultrasound frequency increases the number of active cavitation bubbles [11]. The decrease in the H_2O_2 yield when the frequency is increased from 585 to 1140 kHz may be due to the relatively less time available during the expansion phase of the bubble growth. At relatively high frequencies, the acoustic cycle becomes very short, which restricts the amount of water vapor that can evaporate into the bubble during the expansion phase of the acoustic cycle. A decrease of the amount of water vapor within the collapsing bubble leads to a decrease of the amount of H_2O_2 radicals generated.

4.2. Relationship between bubble dynamics and chemical bubble yield

The key parameter for knowing how acoustic bubbles induce chemical yield is the dynamic of the bubble under an acoustical field. An analysis of the bubble radius variation as function of time (the fit, using our model, and the data from the work of Ohl et al. [49]) was given in our recent paper [50] for typical sonoluminescing bubble trapped at 21.4 kHz. Under the experimental conditions of Ohl et al. [49], the predicted evolution of bubble core temperature and the reaction system inside a bubble is shown in Fig. 2.

In O_2-satured water, the main bubble contents are oxygen and water vapor. During the final stage of the bubble collapse, the bubble content is heated up to 4000 K (Fig. 2), which can promote chemical reactions inside a bubble (Fig. 2). Oxygen and water vapor molecules trapped in the bubble are dissociated and many chemical products such as H_2, H_2O_2, $HO_2^{\cdot}$, $H^{\cdot}$, O and $^{\cdot}OH$ are created in time scale of ~0.1 μs. Because of the short reaction time (~0.1 μs) and the high reactivity of the radical species, it is impossible to make experimental evidence of the computational results, particularly those of Fig. 2. From Fig. 2, it seems that among all the oxidants, only $^{\cdot}OH$ radicals are formed in the bubble at appreciable amounts. Hydrogen peroxide, H_2O_2, has not seen to be formed in the bubble at appreciable amount because at higher temperature H_2O_2 is unstable and dissociates rapidly inside a bubble by the reaction $H_2O_2 + M \rightarrow 2^{\cdot}OH + M$ [29]. The amount of each chemical species attained their upper limit at the end of the bubble collapse (at $R = R_{min}$), followed by almost constant evolution after the end of the bubble collapse as the temperature inside a bubble decreases suddenly. Similar behavior has been obtained by Yasui et al. [39,51] using a more detailed model. In the following sections, the number of moles of each active species (particularly $n_{^{\cdot}OH}$, $n_{HO_2^{\cdot}}$ and $n_{H_2O_2}$) released by each bubble is defined as that obtained at the end of the bubble collapse, when the implosion velocity is null (at $R = R_{min}$).

Table 4
Maximum bubble radius R_{max}, bubble lifetime and acoustic period as function of ultrasonic frequency, under our experimental conditions. R_{max} and bubble lifetime were obtained during the solving of the bubble dynamic equation (Eq. (3)). The acoustic period is the inverse of the ultrasonic frequency [$=1/f$(Hz)].

Frequency (kHz)	Maximum bubble radius R_{max} (μm)	Bubble life time (μs)	Acoustic period (μs)
300	16.79	2.97	3.33
585	9.31	1.57	1.71
860	6.51	1.08	1.16
1140	3.93	0.73	0.87

4.3. Number of collapsing bubbles

According to experimental [52–57] and theoretical data [24,58,59], it is known that the ambient radius (R_0) for a typical active bubble depends on the experimentally controllable parameters such as the driving ultrasonic frequency. Brotchie et al. [23] determined in one of the most extensive investigation that the initial size of active bubbles (R_0) in a cavitating medium is not a single value whereas it has a range. There is a certain size of ambient bubble radii (R_0) at which a dominant number of bubbles was observed in the cavitation region. This size represents the mean ambient radius of active bubbles in sonochemical reaction. Additionally, experiments [23,52,55,57] showed that the range of ambient radius for active bubbles is rather narrow and it closes around the mean ambient radius. Brotchie et al. [23] found that for high frequencies (>200 kHz), the mean ambient radius of active bubbles in a cavitation field decreases with increasing frequency and increases with increasing acoustic amplitude. In our previous work [24], we have studied in detail the effect of ultrasound frequency (in the range of 200–1000 kHz) and acoustic amplitude (up to

Table 3
Experimental and numerical results of the H_2O_2 production rates, the moles number of $^{\cdot}OH$, $HO_2^{\cdot}$ and H_2O_2 released by the collapse of each bubble and the number of collapsing bubbles N with respect to the ultrasonic frequency. The moles number of $^{\cdot}OH$, $HO_2^{\cdot}$ and H_2O_2 released by each bubble were calculated for a bubble initially composed of air and water vapor.

Frequency (kHz)	Production rate of H_2O_2, $r_{H_2O_2}$ (μM min^{-1})	Moles number			Number of bubbles N (L^{-1} s^{-1})
		$n_{^{\cdot}OH}$	$n_{HO_2^{\cdot}}$	$n_{H_2O_2}$	
300	2.5071	3.07×10^{-15}	4.71×10^{-17}	4.67×10^{-18}	2.8428×10^{7}
585	4.2060	4.50×10^{-16}	6.45×10^{-18}	9.95×10^{-19}	3.9433×10^{8}
860	3.4386	5.44×10^{-17}	7.16×10^{-19}	1.03×10^{-19}	3.0414×10^{9}
1140	2.0960	3.28×10^{-17}	4.88×10^{-19}	7.18×10^{-20}	3.0787×10^{9}

Table 5
Experimental and numerical results of the H_2O_2 production rates, the moles number of ·OH, $HO_2^·$ and H_2O_2 released by each bubble at the end of the bubble collapse and the number of collapsing bubbles N with respect to the ultrasonic frequency under the experimental conditions of Pétrier and Francony [19] and Jang et al. [63]. The moles number of ·OH, $HO_2^·$ and H_2O_2 released by each bubble were calculated for an O_2/water vapor bubbles.

Frequency (kHz)	Rate of H_2O_2 production, $r_{H_2O_2}$ (μM/min)		Moles number			Number of bubbles N (L^{-1} s^{-1})	
	Pétrier and Francony	Jiang et al.	$n_{·OH}$	$n_{HO_2^·}$	$n_{H_2O_2}$	Pétrier and Francony	Jiang et al.
20	0.7	1.1	3.09×10^{-12}	1.04×10^{-13}	8.95×10^{-15}	7.2705×10^{3}	1.1425×10^{4}
200	5	5.2	3.06×10^{-14}	1.09×10^{-15}	8.52×10^{-17}	5.2249×10^{6}	5.4339×10^{6}
500	2.1	3	1.80×10^{-15}	6.49×10^{-17}	5.19×10^{-18}	3.7309×10^{7}	5.3299×10^{7}
800	1.4	2	7.01×10^{-16}	2.53×10^{-17}	2.02×10^{-18}	6.3908×10^{7}	9.1297×10^{7}

3 atm) on the size (in term of R_0) of active bubbles using the same model described in Section 3. We found that there exist an optimum ambient bubble radius (R_0) which maximizes the sonochemical production of radicals in the bubble. This optimal value of R_0, which represents the typical radius of active bubbles, is in excellent agreement with the mean ambient bubble radius determined experimentally and it increased with increasing acoustic amplitude and decreased with increasing frequency, agreeing well with the general trend observed experimentally [24,56].

For our experimental conditions, the mean ambient bubble radius (the typical R_0 for active bubbles) for the numerical simulation of the bubble oscillation was selected according to the experimental determinations as 5 μm for 300 kHz [56,60], 3.5 μm for 585 kHz [23], 2.7 μm at 860 kHz [23] and 1.4 μm at 1140 kHz [23,57].

Table 3 summarizes the experimental and numerical results of the H_2O_2 production rates, the mole numbers of ·OH, $HO_2^·$ and H_2O_2 released by each bubble at the end of the bubble collapse and the number of collapsing bubbles N with respect to the ultrasonic frequency.

As can be seen from Table 3, millions of bubbles are formed in the reactor during sonication. The number of active bubbles increases substantially as the ultrasonic frequency increases. Although this trend is in line with the one reported in the literature [20,60], a direct comparison is not possible because most existing literature results [54,56,61,62] were obtained from experimental conditions, i.e. frequency, acoustic intensity and liquid temperature and volume, that are different from those used in our study.

The obtained trend of increasing bubbles number N with increasing frequency of ultrasound can be interpreted as follows: during expansion phase, the bubble will reach a maximum size (R_{max}) immediately before implosion. The maximum size R_{max} of the bubble is inversely correlated to the emitted frequency and is given under our experimental conditions with the bubble lifetime and the acoustic period in Table 4. As frequency increases, the maximum size of the bubbles decreases and, correspondingly, bubble lifetimes decrease as well (Table 4). Assuming that active bubbles are fragmented into daughter bubbles during one acoustic cycle (the bubble lifetime is more than 90% of the acoustic period as indicated in Table 4) the expansion and the collapse of bubbles occur rapidly as the frequency of ultrasound increases due to the shorter acoustic period at higher frequency (Table 4). This leads to a faster rate of bubbles production because the number of cycles per second is higher at higher frequency. Probably, this is the reason for the rise of the number of active bubbles N with the rise of ultrasound frequency.

The number of collapsing bubbles N was also predicted under the conditions of the experiments of Pétrier and Francony [19] and Jiang et al. [63] which studied the effect of ultrasonic frequency (in the range 20–800 kHz) on the sonochemical production of H_2O_2 in an O_2-saturated water. In these experiments, the acoustic power supplied to the sonicators is 30 W (P_a = 2.6 atm), as determined calorimetrically, and the liquid temperature is 20 °C. For these two literature experiments, the typical ambient radius of active bubbles (R_0) was also selected as function of frequency according to experimental determinations. For 20 kHz, active bubbles have a typical radius of 8 μm as determined by Laser light diffraction by Burdin et al. [64] and Tsochatzidis et al. [65], which also determined that the value of 8 μm is not changed for a wide range of acoustic power (20–320 W). The other selected values of R_0 are: 8 μm for 200 kHz [53], 3 μm for 500 kHz [55] and 2.7 μm for 800 kHz [23].

Table 5 shows the experimental and numerical results of the H_2O_2 production rates and the number of bubbles N with respect to the ultrasonic frequency under the experimental conditions of Pétrier and Francony [19] and Jiang et al. [63]. The results of Table 5 confirm the trend of increasing bubbles number with increasing frequency although the change in the operational conditions between our experiments, which are conducted under air-atmosphere at 25 °C when the optimum frequency is 585 kHz, and the experiments of Pétrier and Francony and Jiang et al. performed under O_2-atmosphere at 20 °C when the optimum frequency is 200 kHz. This difference in operational conditions affects necessarily both the experimental production rate of H_2O_2 and the predicted number of moles of the oxidants created in the bubble, as shown in Tables 3 and 5.

5. Conclusion

In the present paper, a simple semi-empirical method for the prediction of the number of active bubbles in acoustic cavitating field have been developed. In one part, the overall sonochemical production of H_2O_2 in cavitating water is determined experimentally at different conditions. In the other part, the chemical yield (particularly, the amounts of ·OH, $HO_2^·$ and H_2O_2) produced by single bubble has been predicted using a model that combines the bubble dynamics in acoustic field with a chemical kinetics model. Exploiting that H_2O_2 content determined experimentally during water sonolysis comes from the recombination of hydroxyl (·OH) and perhydroxyl ($HO_2^·$) radicals at the liquid interface of all bubbles, the number of bubbles formed in the cavitating medium is then easily determined using material balances for H_2O_2, ·OH and $HO_2^·$ in the liquid phase. The effect of ultrasonic frequency on the number of active bubbles was examined. It is shown that increasing ultrasonic frequency leads to a substantial increase in the number of bubbles formed in the reactor. Finally, the present study provides a method that is easy to manipulate and that can give a prediction of the number of bubble for large interval of experimental conditions of frequency, contrary to the most reported method in the literature, which are complicated and treat only some isolated cases (individual frequency).

Acknowledgement

The financial support by the Ministry of Higher Education and Scientific Research of Algeria (project No. J0101120120098) is greatly acknowledged.

References

[1] M.R. Hoffmann, I. Hua, R. Höchemer, Application of ultrasonic irradiation for the degradation of chemical contaminants in water, Ultrason. Sonochem. 3 (1996) S163–S172.
[2] C. Pétrier, Y. Jiang, M.-F. Lamy, Ultrasound and environment: sonochemical destruction of chloroaromatic derivatives, Environ. Sci. Technol. 32 (1998) 1316–1318.
[3] P.R. Gogate, A.B. Pandit, A review of imperative technologies for wastewater treatment II: hybrid methods, Adv. Environ. Res. 8 (2004) 553–597.
[4] T.J. Mason, J.P. Lorimer, Applied Sonochemistry: the Use of Power Ultrasound in Chemistry and Processing, Wiley-VCH Verlag GmbH, Weinheim, 2002. pp. 198–214.
[5] A. Gedanken, Using sonochemistry for the fabrication of nanomaterials, Ultrason. Sonochem. 11 (2004) 47–55.
[6] K. Okitsu, M. Ashokkumar, F. Grieser, Sonochemical synthesis of gold nanoparticles: effects of ultrasound frequency, J. Phys. Chem. B 109 (2005) 20673–20675.
[7] T.J. Mason, L. Paniwnyk, J.P. Lorimer, The uses of ultrasound in food technology, Ultrason. Sonochem. 3 (1996) S253–S260.
[8] D. Bermúdez-Aguirre, T. Mobbs, G.V. Barbosa-Cánovas, Ultrasound applications in food processing, in: H. Feng, G. Barbosá-Canovas, J. Weiss (Eds.), Ultrasound Technology for Food and Bioprocessing, Springer, New York, 2011, pp. 65–105. Chap. 3.
[9] T. Yu, Z. Wang, T.J. Mason, A review of research into the use of low level ultrasound in cancer therapy, Ultrason. Sonochem. 11 (2004) 95–103.
[10] T. Yu, S. Li, J. Zhao, T.J. Mason, Ultrasound: a chemotherapy sensitizer, Technol. Cancer Res. Treat. 5 (2006) 51–60.
[11] T.G. Leighton, The Acoustic Bubble, Academic press, London, UK, 1994.
[12] S.J. Putterman, K.R. Weninger, Sonoluminescence: how bubbles turn sound into light, Ann. Rev. Fluid Mech. 32 (2000) 445–476.
[13] K.S. Suslick, D.J. Flannigan, Inside a collapsing bubble: sonoluminescence and the conditions during cavitation, Annu. Rev. Phys. Chem. 59 (2008) 659–683.
[14] K. Yasui, Fundamental of acoustic cavitation and sonochemistry, in: Pankaj, M. Ashokkumar (Eds.), Theoretical and experimental sonochemistry involving inorganic systems, Springer, London, 2010, pp. 2–5. chap. 1.
[15] K.S. Suslick, D.A. Hammerton, R.E.J. Cline, Sonochemical hotspot, J. Am. Chem. Soc. 108 (1986) 5641–5642.
[16] L.H. Thompson, L.K. Doraiswamy, Sonochemistry: science and engineering, Ind. Eng. Chem. Res. 38 (1999) 1215–1249.
[17] P. Riesz, D. Berdahl, C.L. Christman, Free radical generation by ultrasound in aqueous and nonaqueous solutions, Environ. Health Perspect. 64 (1985) 233–252.
[18] Y.G. Adewuyi, Sonochemistry: environmental science and engineering applications, Ind. Eng. Chem. Res. 40 (2001) 4681–4715.
[19] C. Pétrier, A. Francony, Ultrasonic wastewater treatment: incidence of ultrasonic frequency on the rate of phenol and carbon tetrachloride degradation, Ultrason. Sonochem. 4 (1997) 295–300.
[20] P. Kanthale, F. Ashokkumar, F. Grieser, Sonoluminescence, sonochemistry (H_2O_2 yield) and bubble dynamics: frequency and power effects, Ultrason. Sonochem. 15 (2008) 143–150.
[21] S. Merouani, O. Hamdaoui, F. Saoudi, M. Chiha, Influence of experimental parameters on sonochemistry dosimetries: KI oxidation, Fricke reaction and H_2O_2 production, J. Hazard. Mater. 187 (2010) 1007–1014.
[22] K.S. Suslick, Y. Didenko, M.M. Fang, T. Hyeon, K.J. Kolbeck, W.B. McNamara, M.M. Mdleleni, M.M. Wong, Acoustic cavitation and its chemical consequences, Philos. Trans. R. Soc. A: Math. Phys. Eng. Sci. 357 (1999) 335–353.
[23] A. Brotchie, F. Grieser, M. Ashokkumar, Effect of power and frequency on bubble-size distributions in acoustic cavitation, Phys. Rev. Lett. 102 (2009) 084302.
[24] S. Merouani, O. Hamdaoui, Y. Rezgui, M. Guemini, Effects of ultrasound frequency and acoustic amplitude on the size of sonochemically active bubbles – theoretical study, Ultrason. Sonochem. 20 (2013) 815–819.
[25] S. Koda, T. Kimura, T. Kondo, H. Mitome, A standard method to calibrate sonochemical efficiency of an individual reaction system, Ultrason. Sonochem. 10 (2003) 149–156.
[26] T.J. Mason, J.P. Lorimer, D.M. Bates, Quantifying sonochemistry: casting some light on a 'black art', Ultrasonics 30 (1992) 40–42.
[27] C. Kormann, D.W. Bahnemann, M.R. Hoffmann, Photocatalytic production of H_2O_2 and organic peroxides in aqueous suspensions of TiO_2, ZnO, and desert sand, Environ. Sci. Technol. 22 (1988) 798–806.
[28] S. Merouani, O. Hamdaoui, Y. Rezgui, M. Guemini, Computer simulation of chemical reactions occurring in collapsing acoustical bubble: dependence of free radicals production on operational conditions, Res. Chem. Intermed. (in press) (2013), doi: 10.1007/s11164-013-1240-y.
[29] S. Merouani, O. Hamdaoui, Y. Rezgui, M. Guemini, Theoretical estimation of the temperature and pressure within collapsing acoustical bubbles, Ultrason. Sonochem. 21 (2014) 53–59.
[30] S. Merouani, O. Hamdaoui, Y. Rezgui, M. Guemini, Energy analysis during acoustic bubble oscillations: relationship between bubble energy and sonochemical parameters, Ultrasonics 54 (2014) 227–232.
[31] L.A. Crum, The polytrophic exponent of gas contained within air bubbles pulsating in a liquid, J. Acoust. Soc. Am. 73 (1983) 116–120.
[32] J.B. Keller, I.I. Kolodner, Damping of underwater explosion bubble oscillations, J. Appl. Phys. 27 (1956) 1152–1161.
[33] J.B. Keller, M.J. Miksis, Bubble oscillations of large amplitude, J. Acoust. Soc. Am. 68 (1980) 628–633.
[34] A.J. Colussi, L.K. Weavers, M.R. Hoffmann, Chemical bubble dynamics and quantitative sonochemistry, J. Phys. Chem. A 102 (1998) 6927–6934.
[35] N.P. Vichare, P. Senthilkumar, V.S. Moholkar, P.R. Gogate, A.B. Pandit, Energy analysis in acoustic cavitation, Ind. Eng. Chem. Res. 39 (2000) 1480–1486.
[36] B.D. Storey, A.J. Szeri, Water vapor, sonoluminescence and sonochemistry, Proc. R. Soc. London A 456 (2000) 1685–1709.
[37] V. Kamath, A. Prosperetti, F.N. Egolfopoulos, A theoretical study of sonoluminescence, J. Acoust. Soc. Am. 94 (1993) 248–260.
[38] K. Yasui, A new formulation of bubble dynamics for sonoluminescence (PhD thesis) Waseda University, Japan, 1996.
[39] K. Yasui, T. Tuziuti, Y. Iida, H. Mitome, Theoretical study of the ambient-pressure dependence of sonochemical reactions, J. Chem. Phys. 119 (2003) 346–356.
[40] R. Toegel, D. Ioshe, Phase diagrams for sonoluminescing bubbles: a comparison between experiment and theory, J. Chem. Phys. 118 (2003) 1863–1875.
[41] B.-S. Choi, J.S. Oh, S.-W. Lee, H. Kim, J. Yi, Simulation of the effects of CCl_4 on the ethylene dichloride pyrolysis process, Ind. Eng. Chem. Res. 40 (2001) 4040–4049.
[42] W.M. Nelson, I.K. Puri, Oxidation of CH_3CHO by O_3 and H_2O_2 mixtures in supercritical CO_2 in a perfectly stirred reactor, Ind. Eng. Chem. Res. 36 (1997) 3446–3452.
[43] NIST Chemical Kinetics Database (2011), <http://kinetics.nist.gov/kinetics/index.jsp>.
[44] D.L. Baulch, C.J. Cobos, R.A. Cox, C. Esser, P. Frank, Th. Just, J.A. Kerr, M.J. Pilling, J. Troe, R.W. Walker, J. Warnatz, Evaluated kinetic data for combustion modelling, J. Phys. Chem. Ref. Data 21 (1992) 411–734.
[45] T. Sivasankar, A.W. Paunikar, V.S. Moholkar, Mechanistic approach to enhancement of the yield of a sonochemical reaction, AIChE 53 (2007) 1132–1143.
[46] D.V. Prasad Naidu, R. Rajan, R. Kumar, K.S. Gandhi, V.H. Arakeri, S. Chandrasekaran, Modelling of a batch sonochemical reactor, Chem. Eng. Sci. 49 (1994) 877–888.
[47] T.P.A. Devasagayam, J.C. Tilak, K.K. Boloor, K.S. Sane, S.S. Ghaskadbi, R.D. Lele, Free radicals and antioxidants in human health: current status and future prospects, JAPI 52 (2004) 794–804.
[48] J.B.D. Heredia, J. Torregrosa, J.R. Dominguez, J.A. Peres, Kinetic model for phenolic compound oxidation by Fenton's reagent, Chemosphere 45 (2001) 85–90.
[49] C. Ohl, T. Kurz, R. Geisler, O. Lindau, W. Lauterborn, Bubble dynamics, shock waves and sonoluminescence, Philos. Trans. R. Soc. London A 357 (1999) 269–294.
[50] S. Merouani, O. Hamdaoui, Y. Rezgui, M. Guemini, Theoretical procedure for the characterization of acoustic cavitation bubbles, Acta Acust. United Acust. (2014), (accepted manuscript).
[51] K. Yasui, T. Tuziuti, M. Sivakumar, Y. Iida, Theoretical study of single-bubble sonochemistry, J. Chem. Phys. 122 (2005) 224706.
[52] S. Xu, Y. Zong, W. Li, S. Zhang, M. Wan, Bubble size distribution in acoustic droplet vaporization via dissolution using an ultrasound wide-beam method, Ultrason. Sonochem. 21 (2014) 975–983.
[53] A. Thiemann, T. Nowak, R. Mettin, F. Holsteyns, A. Lippert, Characterization of an acoustic cavitation bubble structure at 230 kHz, Ultrason. Sonochem. 18 (2011) 595–600.
[54] Y. Iida, M. Ashokkumar, T. Tuziuti, T. Kozuka, K. Yasui, A. Towada, J. Lee, Bubble population phenomena in sonochemical reactor: estimation of bubble size distribution and its number density with pulsed sonication – laser diffraction method, Ultrason. Sonochem. 17 (2010) 473–479.
[55] J. Lee, M. Ashokkumar, S. Kentish, F. Grieser, Determination of the size distribution of sonoluminescence bubbles in a pulsed acoustic field, J. Am. Chem. Soc. 127 (2005) 16810–16811.
[56] S. Labouret, J. Frohly, Distribution en tailles des bulles d'un champ de cavitation ultrasonore, 10ème Congrès Français d'Acoustique, 2010.
[57] W.-S. Chen, T.J. Matula, L.A. Crum, The disappearance of ultrasound contrast bubbles: observations of bubble dissolution and cavitation nucleation, Ultrasound Med. Biol. 28 (2002) 793–803.
[58] K. Yasui, Influence of ultrasonic frequency on multibubble sonoluminescence, J. Am. Chem. Soc. 112 (2002) 1405–1413.
[59] K. Yasui, T. Tuziuti, J. Lee, T. Kozuka, A. Towada, The range of ambient radius for an active bubble in sonoluminescence and sonochemical reactions, J. Chem. Phys. 128 (2008) 184705.
[60] A. Brotchie, F. Grieser, M. Ashokkumar, Characterization of acoustic cavitation bubbles in different sound fields, J. Chem. Phys. B 114 (2010) 11010–11016.
[61] S. Labouret, J. Frohly, Bubble size distribution estimation via void rate dissipation in gas saturated liquid. Application to ultrasonic cavitation bubble fields, Eur. Phys. J. Appl. Phys. 19 (2002) 39–54.
[62] B. Avvaru, A.B. Pandit, Oscillating bubble concentration and its size distribution using acoustic emission spectra, Ultrason. Sonochem. 16 (2009) 105–115.
[63] Y. Jiang, C. Petrier, T.D. Waite, Sonolysis of 4-chlorophenol in aqueous solution: effects of substrate concentration, aqueous temperature and ultrasonic frequency, Ultrason. Sonochem. 13 (2006) 415–422.
[64] F. Burdin, N.A. Tsochatzidis, P. Guiraud, A.M. Wilhelm, H. Delmas, Characterization of the acoustic cavitation cloud by two laser techniques, Ultrason. Sonochem. 6 (1999) 43–51.
[65] N.A. Tsochatzidis, P. Guiraud, A. Wilhelm, H. Delmas, Determination of velocity, size and concentration of ultrasonic cavitation bubbles by the phase-Doppler technique, Chem. Eng. Sci. 56 (2001) 1831–1840.